

HALO CONCENTRATIONS AND THE NEW BASELINE X-RAY LUMINOSITY-TEMPERATURE AND MASS RELATIONS OF GALAXY CLUSTERS

YUTAKA FUJITA¹, HAN AUNG²

¹Department of Earth and Space Science, Graduate School of Science, Osaka University, Toyonaka, Osaka 560-0043, Japan

²Department of Physics, Yale University, New Haven, CT 06520, USA

(Received January 1, 0000; Revised January 1, 0000; Accepted April 12, 2019)

Draft version April 12, 2019

ABSTRACT

The standard self-similar model of galaxy cluster formation predicts that the X-ray luminosity–temperature (L_X – T_X) relation of galaxy clusters should have been $L_X \propto T_X^2$ in absence of the baryonic physics, such as radiative cooling and feedback from stars and black holes. However, this baseline relation is predicted without considering the fact that the halo concentration and the characteristic density of clusters increases as their mass decreases, which is a consequence of hierarchical structure formation of the universe. Here, we show that the actual baseline relation should be $L_X \propto T_X^\alpha$, where $\alpha \sim 1.7$, instead of $\alpha = 2$, given the mass dependence of the concentration and the fundamental plane relation of galaxy clusters. Numerical simulations show that $\alpha \sim 1.6$, which is consistent with the prediction. We also show that the baseline luminosity–mass (L_X – M_Δ) relation should have been $L_X \propto M_\Delta^\beta$, where $\beta \sim 1.1$ – 1.2 , in contrast with the conventional prediction ($\beta = 4/3$). In addition, some of the scatter in the L_X – M_Δ relation can be attributed to the scatter in the concentration–mass (c – M) relation. The confirmation of the shallow slope could be a proof of hierarchical clustering. As an example, we show that the new baseline relations could be checked by studying the temperature or mass dependence of gas mass fraction of clusters. Moreover, the highest-temperature clusters would follow the shallow baseline relations if the influences of cool cores and cluster mergers are properly removed.

Subject headings: galaxies: clusters: general — galaxies: clusters: intracluster medium — cosmology: observations — X-rays: galaxies: cluster

1. INTRODUCTION

Clusters of galaxies have grown from slightly overdense regions of the universe. The initial density fluctuations of the universe are described by a random Gaussian field with a power spectrum having a smoothly changing power-law index. Thus, clusters are expected to have a high degree of self-similarity in scale and time, which leads to various scaling relations among observables, although the relations may be affected by the mass assembly histories of dark matter halos. The relation between the X-ray luminosity L_X and temperature T_X of clusters has been studied for many years, probably because it is relatively easy to measure them. Observations have shown that the relation is approximately described as $L_X \propto T_X^3$ (e.g. Edge & Stewart 1991; Markevitch 1998). This relation is thought to be influenced by feedback from active galactic nuclei (AGNs) and supernovae in galaxies in clusters (e.g. Voit et al. 2002; Borgani et al. 2004; Puchwein et al. 2008). The relation when there was no feedback is often expected to be $L_X \propto T_X^2$ (Kaiser 1986; Bryan & Norman 1998). We refer to scaling relations when there were no nongravitational effects (e.g. feedback and radiative cooling) as the “baseline relations,” because they are used as baselines when the nongravitational effects are estimated.

The conventional baseline relation of $L_X \propto T_X^2$ is derived assuming that cluster structure is self-similar and the characteristic density of clusters is proportional to the density of the background universe. This means that

clusters at a given redshift have a common characteristic density. However, this assumption seems to be at odds with recent studies on structure formation of the universe. Numerical simulations have shown that the dark matter density profile of galaxy clusters is well represented by the Navarro–Frenk–White (NFW) density profile (Navarro et al. 1997), and that less massive clusters tend to be more concentrated and have higher characteristic densities. In other words, the characteristic density differs among clusters even at a given redshift. This is because in the standard CDM cosmology, less massive clusters form earlier and their characteristic density reflects the higher background density of the universe at their formation time (e.g. Navarro et al. 1997; Wechsler et al. 2002; Zhang et al. 2008; Ludlow et al. 2013). Thus, their mass dependence is a consequence of hierarchical structure formation of the universe (e.g. Duffy et al. 2008; Bhattacharya et al. 2013; Meneghetti et al. 2014).

Scaling relations for clusters are not necessarily limited to one-to-one correlations. For example, relations among three parameters are often considered and “fundamental planes” are the representative ones (Schaeffer et al. 1993; Adami et al. 1998; Fujita & Takahara 1999; Verde et al. 2002; Lanzoni et al. 2004; Ota et al. 2006; Araya-Melo et al. 2009; Ettori 2013; Maughan 2014; Ettori 2015). Recently, Fujita et al. (2018a, see Fujita et al. 2019 for a review) found that observed clusters are distributed on a plane in the space of $(\log r_s, \log M_s, \log T_X)$, where r_s and M_s are the characteristic radius and mass for the NFW profile, respectively, and T_X is the X-ray temperature. Numerical simulations have confirmed the plane

and have shown that clusters evolve along the plane. Thus, this fundamental plane reflects the structure and evolution of dark matter halos of clusters. The non-gravitational effects and cluster mergers have little effect on the plane. The properties of the plane can be explained by an analytical model of structure formation constructed by Bertschinger (1985). In particular, the angle of the plane in the space of $(\log r_s, \log M_s, \log T_X)$ indicates that clusters have not perfectly achieved virial equilibrium because of continuous matter accretion from the surroundings (Fujita et al. 2018a). We note that the deviation from the virial equilibrium is not considered when the conventional relation $L_X \propto T_X^2$ is constructed.

In this study, we revise the baseline L_X – T_X relation considering the mass dependence of the halo concentrations and the fundamental plane. We also study the baseline luminosity–mass (L_X – M_Δ) relation as a corollary. The paper is organized as follows. In Section 2, we review the derivation of the conventional baseline relations. In Section 3, we derive the revised baseline L_X – T_X and L_X – M_Δ relations by taking into account the mass dependence of halo concentrations and the fundamental plane relation, and show that they deviate from the conventional relations. In Section 4, we test the predictions of our new model using the *Omega500* hydrodynamical cosmological simulations of galaxy cluster formation. In Section 5, we discuss future observations of the L_X – T_X and L_X – M_Δ relations. In Section 6, we summarize our main results.

In this paper, we assume a spatially flat Λ CDM cosmology with $\Omega_m = 0.27$, $\Omega_\Lambda = 0.73$, and the Hubble constant of $H_0 = 100 h \text{ km s}^{-1} \text{ Mpc}^{-1}$ for $h = 0.7$, unless otherwise mentioned.

2. CONVENTIONAL BASELINE RELATIONS

The conventional scaling relations are based on a gravitational collapse model of a homogeneous spherical overdense region in the Einstein-de Sitter universe (Kaiser 1986). This region initially expands with the Hubble expansion. Then, owing to the gravity, it deviates from the expansion, and starts to collapse. The evolution is self-similar and can be treated analytically (e.g. Peebles 1980). If the collapsed region is virialized, the average density is $18\pi^2 \sim 200$ times the critical density of the universe. Subsequent matter accretion from the surroundings is not considered in this model.

The conventional baseline relation of $L_X \propto T_X^2$ can be derived as follows. First, we assume that the typical density of clusters is $\rho_\Delta \equiv \Delta \rho_c(z)$, where Δ is a constant and $\rho_c(z)$ is the critical density of the universe at redshift z . The critical density depends on z as in $\rho_c(z) \propto E(z)^2$, where the Hubble parameter at z is represented by $H(z) = H_0 E(z)$ and H_0 is the Hubble constant. The density ρ_Δ does not depend on clusters and is constant at a given redshift. The corresponding cluster radius r_Δ is defined as the one inside which the average density is ρ_Δ , and the mass is written as

$$M_\Delta = \frac{4\pi}{3} \rho_\Delta r_\Delta^3. \quad (1)$$

For the overdensity, $\Delta = 200$ is often used because it is close to $18\pi^2$. However, it is generally difficult to observe cluster properties out to r_{200} ; $\Delta = 500$ is also often used.

Assuming that the cooling function of the intracluster medium (ICM) is described by bremsstrahlung, the bolometric emissivity is proportional to $\rho_{\text{ICM}}^2 T_X^{1/2}$, where ρ_{ICM} is the typical density of the ICM. Here, we assume that $\rho_{\text{ICM}} \propto \rho_\Delta$. Since the typical volume of a cluster is proportional to r_Δ^3 , the X-ray luminosity of clusters is represented by

$$L_X \propto \rho_\Delta^2 T_X^{1/2} r_\Delta^3. \quad (2)$$

If we assume the virial equilibrium, the X-ray temperature is given by $T_X \propto M_\Delta / r_\Delta \propto \rho_\Delta r_\Delta^2$ using equation (1). Considering that $\rho_\Delta \propto E(z)^2$ and $r_\Delta \propto T_X^{1/2} E(z)^{-1}$, we finally obtain the relation of

$$L_X \propto T_X^2 E(z) \quad (3)$$

from equation (2) (Kaiser 1986; Bryan & Norman 1998). Thus, $L_X \propto T_X^2$ for a given z . Similarly, the baseline luminosity–mass relation can be obtained as in $L_X \propto M_\Delta^{4/3} E(z)^{7/3}$ (Bryan & Norman 1998).

3. NEW BASELINE RELATIONS

However, the above derivations do not take into account the mass profile of clusters. Numerical simulations have shown that the dark matter density profile of galaxy clusters is well represented by the NFW density profile (Navarro et al. 1997):

$$\rho_{\text{DM}}(r) = \frac{\delta_c \rho_c}{(r/r_s)(1+r/r_s)^2}, \quad (4)$$

where r is the cluster centric radius, r_s is the characteristic radius, and δ_c is the normalization. The radius r_s is smaller than r_Δ for clusters if $\Delta = 200$ and 500. We define the characteristic mass M_s as the mass enclosed within $r = r_s$, and define the characteristic density as $\rho_s \equiv 3 M_s / (4\pi r_s^3)$. The halo concentration parameter is given by

$$c_\Delta = r_\Delta / r_s. \quad (5)$$

The mass profile of the NFW profile is then given by

$$M(r) = 4\pi \delta_c \rho_c r_s^3 \left[\ln \left(1 + \frac{r}{r_s} \right) - \frac{r}{r+r_s} \right]. \quad (6)$$

From this equation, the characteristic mass M_s can be expressed in terms of M_Δ and c_Δ :

$$M_s = M_\Delta \frac{\ln 2 - 1/2}{\ln(1+c_\Delta) - c_\Delta/(1+c_\Delta)}. \quad (7)$$

N -body simulations have shown that $c_\Delta = c_\Delta(M_\Delta, z)$ is a decreasing function of M_Δ for a given z , with a considerable dispersion (~ 0.1 dex) due to the diversity in cluster ages for a given mass (e.g. Duffy et al. 2008; Bhattacharya et al. 2013; Meneghetti et al. 2014; Fujita et al. 2018b). While a wide mass range of halos have concentration of $c_{200} \sim 3$ at high redshifts, only most massive halos have $c_{200} \sim 3$ and others have higher concentration at $z \sim 0$ (Child et al. 2018). As a result, from equations (1) and (5), the scale radius $r_s \propto (M_\Delta / \rho_\Delta(z))^{1/3} / c_\Delta(M_\Delta, z)$ and the characteristic density $\rho_s = 3 M_s / (4\pi r_s^3)$ also depend on M_Δ and z .

Since the emissivity of the ICM is proportional to the density squared, the X-ray luminosity of clusters should

reflect the structure of their central region where the density is high. If we assume that the dark matter profile follows the NFW profile (equation (4)) and that the ICM density follows that of dark matter ($\rho_{\text{ICM}} \propto \rho_s$), the characteristic volume of a cluster should be $\propto r_s^3$ and the X-ray luminosity is

$$L_X \propto \rho_s^2 T_X^{1/2} r_s^3, \quad (8)$$

in contrast with equation (2). Since ρ_s depends on M_Δ and z while ρ_Δ is constant for a given z , this fact differentiates equation (8) from equation (2). In other words, the variation of the halo concentration among clusters is not considered in the derivation of equation (3). As clusters with larger M_Δ tend to have larger T_X , we expect that the mass dependence of ρ_s affects the L_X – T_X relation as well as the L_X – M_Δ relation if they are derived from equation (8) (see also Enoki et al. 2001).

The revised baseline L_X – T_X and L_X – M_Δ relations of clusters can be obtained using the mass dependence of the concentration parameter c_Δ and the fundamental plane relation given by

$$T_X = T_{X0} \left(\frac{r_s}{r_{s0}} \right)^{-2} \left(\frac{M_s}{M_{s0}} \right)^{(n+11)/6}, \quad (9)$$

where (r_{s0}, M_{s0}, T_{X0}) is a representative point on the fundamental plane (Fujita et al. 2018a,b).¹ Note that T_X is the core excised temperature. The relation does not depend on z at least $z \lesssim 1$ and indicates that clusters in general have not achieved virial equilibrium (Fujita et al. 2018a). The equation (9) can be derived from the entropy constant given in the similarity solution by Bertschinger (1985); the constant reflects the conservation of the ICM entropy. The relation depends on the spectral index n of the density perturbations of the universe, because the overdense region that later becomes the inner part of a cluster and gives the inner boundary of the solution of Bertschinger (1985) evolves from the density perturbations (Fujita et al. 2018a). Although the index should be $n \sim -2$ at cluster scales (e.g. Eisenstein & Hu 1998; Diemer & Kravtsov 2015), we treat n simply as a parameter here. We assume $n = -2$ and -2.5 , both of which are consistent with observed and simulated fundamental planes (Fujita et al. 2018b). Since equation (9) shows that T_X is a function of r_s and M_s , it is also a function of M_Δ and z .

Although we considered only bremsstrahlung for the cooling function ($\Lambda \propto T_X^{1/2}$) in Section 2 and in equation (8) for simplicity and illustration, we will now include the effect of metal-line cooling, which introduces additional dependence on the ICM metallicity Z . The X-ray luminosity would then be given by $L_X \propto n_e^2 \Lambda(T_X, Z) V_{\text{rs}} \propto \rho_s^2 \Lambda(T_X, Z) V_{\text{rs}}$, where $V_{\text{rs}} = (4\pi/3)r_s^3$ and we adopt the following metallicity-dependent cooling function Λ given by

$$\Lambda(T_X, Z) = 2.41 \times 10^{-27} \left[0.8 + 0.1 \left(\frac{Z}{Z_\odot} \right) \right] \left(\frac{T_X}{\text{K}} \right)^{0.5}$$

¹ We use $r_{s0} = 414$ kpc, $M_{s0} = 1.4 \times 10^{14} M_\odot$, and $T_{X0} = 3.7$ keV based on the results of the MUSIC simulations (Meneghetti et al. 2014; Fujita et al. 2018a).

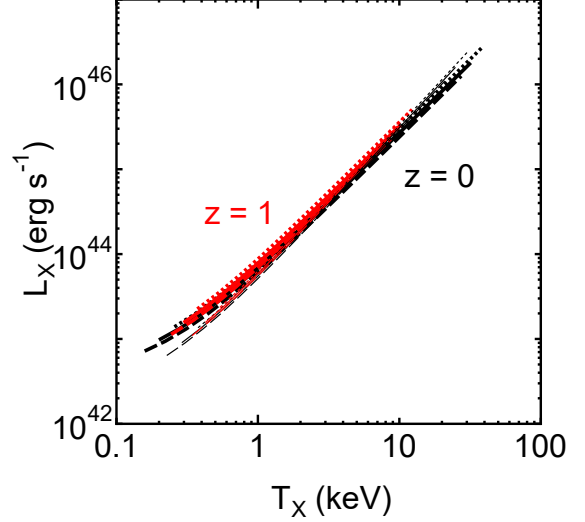


FIG. 1.— L_X – T_X relations for $n = -2$ (thick lines) and $n = -2.5$ (thin lines). Black lines and red lines represent $z = 0$ and 1, respectively. Solid lines are calculated for the fiducial c_Δ – M_Δ relation. The dotted and dashed lines correspond to c_Δ^U and c_Δ^L , respectively. The vertical axis (L_X) is not corrected by $E(z)$.

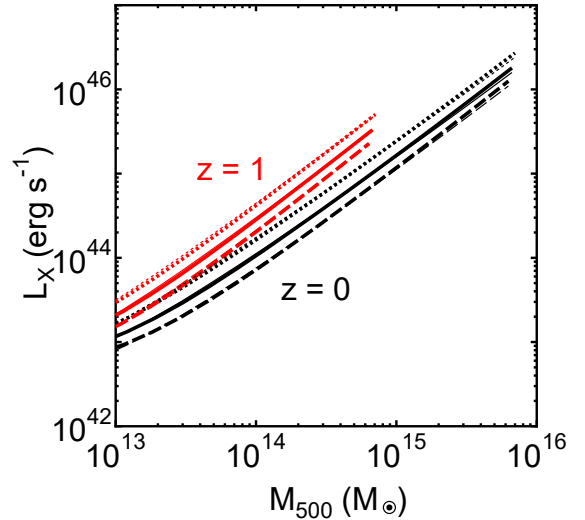


FIG. 2.— Same as Figure 1, but for L_X – M_Δ relations for $\Delta = 500$. Thick and thin lines are almost identical.

$$+ 1.39 \times 10^{-16} \left[0.02 + 0.1 \left(\frac{Z}{Z_\odot} \right)^{0.8} \right] \times \left(\frac{T_X}{\text{K}} \right)^{-1.0} \text{ erg cm}^3 \quad (10)$$

(Fujita & Ohira 2013), which approximates the cooling function derived by Sutherland & Dopita (1993) for $T_X \gtrsim 10^5$ K and $Z \lesssim 1 Z_\odot$.

Now, using M_Δ as a parameter, we can draw the L_X – T_X relation (Figure 1). We assume that $L_X = n_e^2 \Lambda(T_X, 0.3 Z_\odot) V_{\text{rs}}$. Assuming that the ICM consists of hydrogen and helium², the electron density is given by $n_e = 0.86 f_{\text{gas}} \rho_s / m_p$, where m_p is the proton mass and $f_{\text{gas}} = 0.13$ is the gas mass fraction of massive clusters (e.g. Biviano & Salucci 2006; Gonzalez et al. 2013;

² The inclusion of metals have little influence (only a few percent change in n_e) as long as $Z \lesssim 1 Z_\odot$.

Dvorkin & Rephaeli 2015). The solid lines are the fiducial relations that are calculated using the analytic function³ of $c_\Delta = c_\Delta(M_\Delta, z)$ obtained by Correa et al. (2015).

Considering the dispersion of the c_Δ – M_Δ relation, we also represent the L_X – T_X relations when c_Δ (fiducial) is replaced by $c_\Delta^U = 10^{0.1}c_\Delta$ (dotted line) or $c_\Delta^L = 10^{-0.1}c_\Delta$ (dashed line). Figure 1 shows that the solid, dotted, and dashed lines are almost identical, which means that the dispersion of the c_Δ – M_Δ relation does not introduce a scatter in the L_X – T_X relation. Moreover, the L_X – T_X relation does not depend sensitively on redshift, which is in contrast to the relation derived based on the simple self-similar model on a scale of r_Δ (equation (3)). Since the baseline relation does not evolve (Figure 1), observed evolution, if any, can be attributed to additional baryonic physics, such as gas cooling and feedback.

Observationally, there seems to be no consensus about the redshift evolution of the L_X – T_X relation so far (e.g. Böhringer et al. 2012), although Reichert et al. (2011) concluded that the evolution of X-ray luminosity for a given temperature is slower than predicted by a simple self-similar model (see equation 3). Note that the L_X – T_X relation in Figure 1 is constructed from ρ_s and T_X , which reflect cluster properties on a scale of r_s . The observed L_X – T_X relation has a larger scatter (~ 0.2 dex; e.g. Maughan et al. 2012) than those shown by the dotted and dashed lines in Figure 1, which suggests that actual X-ray luminosities are impacted by local and/or temporary phenomena around the cluster centers (e.g., AGN feedback in cool cores and/or disruption of the cores by cluster mergers) and that the effects differ among clusters.

Table 1 summarizes the values of the index α of the L_X – T_X relation ($L_X \propto T_X^\alpha$) for different n and a temperature range of $1 < T_X < 10$ keV. For each index, the smaller one is for $z = 0$ and the larger one is for $z = 1$. The index is determined for the fiducial relation (solid lines in Figure 1) but the results are almost unchanged even if we take the dotted or dashed lines. Although the slope of the L_X – T_X relation becomes slightly shallower for $T_X \lesssim 3$ keV due to the metal-line cooling (Figure 1), the magnitude of this effect is quite small. The indices for a temperature range of $3 < T_X < 10$ keV is larger than those for $1 < T_X < 10$ keV only by ~ 0.03 . We, therefore, conclude that the index α should be smaller than two and should be $\alpha \sim 1.6$ – 1.8 if the ICM density profile follows the dark matter profile. The shallower slope is ascribed to the increase in the halo concentration c_Δ and the characteristic density ρ_s for lower temperature (less massive) clusters. We expect that the smaller index

α is realized when additional physics such as feedback, radiative cooling, and disturbance by cluster mergers are ignorable, because the ICM settled in the potential well of the dark matter halo and r_s is the only spatial scale of the NFW profile.

It may be instructive to represent the L_X – T_X relation only by the fundamental plane. From equations (8), (9), and $\rho_s \propto M_s/r_s^3$, we obtain $L_X \propto T_X^{(19+n)/(14+2n)} \rho_s^{(3+n)/(7+n)}$, which is $L_X \propto T_X^{1.7} \rho_s^{0.2}$ for $n = -2$, and $L_X \propto T_X^{1.83} \rho_s^{0.11}$ for $n = -2.5$. This means that the L_X – T_X relation is not sensitive to ρ_s and that the L_X – T_X relation is close to an “edge-on view” of the fundamental plane (see also Fujita & Takahara 1999). Thus, the relation is almost independent of z and has almost no dispersion (Figure 1(a)), even though ρ_s is a function of z and M_Δ .⁴

As L_X is a function of M_Δ and z , the L_X – M_Δ relation can immediately be obtained. Figure 2 shows the L_X – M_Δ relation for $\Delta = 500$. Table 1 reports the index of the relation β ($L_X \propto M_\Delta^\beta$) for a temperature range of $1 < T_X < 10$ keV, where β_{200} and β_{500} are β for $\Delta = 200$ and 500, respectively. For each index, the smallest one is for $z = 0$ and the largest one is for $z = 1$. The indices are determined for the fiducial relations, indicated with the solid lines in Figure 2. The indices for a temperature range of $3 < T_X < 10$ keV is larger than those for $1 < T_X < 10$ keV only by ~ 0.03 . The table shows that $\beta \sim 1.2$, which is slightly smaller than the prediction of the conventional self-similar model ($\beta = 4/3 \approx 1.33$; Section 2). Clusters with $M_{500} \lesssim 10^{14} M_\odot$ host a plasma with an X-ray emission with a relatively larger contribution from metal-line recombination. For a given mass, L_X at $z = 1$ is larger than that at $z = 0$, mainly because the characteristic density ρ_s is larger for the former. In contrast to the L_X – T_X relation, the dispersion of the c_Δ – M_Δ relation scatters the L_X – M_Δ relation (dotted and dashed lines in Figure 2), which indicates that the L_X – M_Δ relation is not an edge-on view of the fundamental plane. Moreover, as is the case of the L_X – T_X relation, the L_X – M_Δ relation is written as $L_X \propto M_s^{(19+n)/12} \rho_s^{4/3}$ when only the fundamental plane relation is used. Since M_s is approximately represented by $M_s \propto M_{500}^{1.1}$ (equation (7)), the luminosity is given by $L_X \propto M_{500}^{1.56} \rho_s^{1.33}$ for $n = -2$, and $L_X \propto M_{500}^{1.51} \rho_s^{1.33}$ for $n = -2.5$. This means that the L_X – M_Δ relation is sensitive to ρ_s and is scattered by the variety.

We note that observationally determined directions of the fundamental plane have some uncertainties caused by observational errors (see the contours in Figure 2 of Fujita et al. 2018a). On the other hand, numerical simulations have shown that the plane is intrinsically thin (~ 0.03 dex; Fujita et al. 2018a) and that the thickness of the plane does not affect the plane normal. However, the plane relation determined by the simulation results has a small deviation from the relation we assumed in equation (9) (see the marks in Figure 2 of Fujita et al. 2018a). They seem to be associated with treatment of cool cores and presence or absence of nongravitational effects. In

TABLE 1
THE PREDICTIONS OF THE INDICES α AND β

n	α	β_{200}^a	β_{500}^b
-2	1.59–1.61	1.17–1.24	1.19–1.26
-2.5	1.74–1.77	1.12–1.20	1.14–1.22

Notes — ^a β for $\Delta = 200$, and ^b β for $\Delta = 500$.

³ <https://bitbucket.org/astroduff/commah>

⁴ The fundamental plane reflects the higher concentration of lower-mass and/or higher-redshift clusters. The function $c_\Delta = c_\Delta(M_\Delta, z)$ approximately defines the evolution track of clusters on the fundamental plane (Figure 2 in Fujita et al. 2018b).

order to estimate the influence of the deviation, we construct fundamental plane relations $T_X = T_X(r_s, M_s)$ for each of the simulation sets (MUSIC, NF0, FB0, and FB1 in Fujita et al. 2018a) instead of equation (9) and derive the indices for the L_X – T_X and the L_X – M_Δ relations. We found that $1.4 \lesssim \alpha \lesssim 1.9$ and $1.1 \lesssim \beta \lesssim 1.4$. These uncertainties motivate us to directly simulate the L_X – T_X and L_X – M_Δ relations in the next section.

4. NUMERICAL SIMULATIONS

In order to confirm the predictions made in the previous section, we analyze the results of the nonradiative version of the *Omega500* hydrodynamical cosmological simulations (Nelson et al. 2014). We do not include radiative cooling and feedback by AGNs and supernovae when we calculate gas dynamics because the purpose of this study is to find the baseline L_X – T_X and L_X – M_Δ relations.

The simulation *Omega500* is run with Adaptive Tree Refinement, an Eulerian code that uses adaptive refinement in space and time (Kravtsov 1999; Kravtsov et al. 2002; Rudd et al. 2008). The softening length is $3.8 h^{-1}$ kpc for both dark matter particles and gas cells in the high-resolution regions. Nonadaptive refinement in mass necessary for resolving cores of the clusters is employed so that the highest mass resolution for the dark matter particles is $m_{\text{DM}} = 1.09 \times 10^9 h^{-1} M_\odot$. The simulation box has a comoving box length of $500 h^{-1}$ Mpc. We select all of the 65 clusters at $z = 0$ with $M_{500} > 3 \times 10^{14} h^{-1} M_\odot$ regardless of dynamical state. We compute the emission-weighted temperature including the core. We kept the core because these simulations are nonradiative and thus do not present cool-core features. The bolometric luminosity L_X and the temperature T_X are derived within a radius r_{500} . This choice of the radius does not affect the results much if the radius is large enough. This is because X-ray emissivity is proportional to density squared and most of the X-ray emission comes from the central region of clusters. The metal abundance is assumed to be $Z = 0.3 Z_\odot$ in the calculation of the luminosity L_X .

In Figure 3, we show the results for the whole sample (filled + open circles). In Figure 3(a), we fit the data in log space with the function $L_X \propto T_X^\alpha$ using BCES orthogonal regression (solid line; Akritas & Bershady 1996). The index for the fit is $\alpha = 1.51 \pm 0.09$ (all uncertainties are quoted at the 1σ confidence level unless otherwise mentioned), which is almost consistent with the prediction for $n = -2$ in Section 3 (Table 1). However, some of the clusters in Figure 3 are merging clusters, for which the ICM profiles are often significantly deviated from the dark matter profiles. Thus, we study the L_X – T_X relation excluding merging clusters. We define merging clusters as those that undergo a merger of mass ratio of at least one-sixth in the past 2 Gyr, which is about a typical relaxation time scale. Figure 3(a) shows that the dispersion of the L_X – T_X relation is reduced if we choose only nonmerging clusters. The result of a fit for the nonmerging clusters is indicated by the dashed line and the index is $\alpha = 1.57 \pm 0.08$. Changing the merger mass ratio limit to one-fifth or one-seventh only shifts the slope within ± 0.02 . Again, the index is consistent with the prediction when $n = -2$ (Table 1), and $\alpha = 2$ is clearly rejected. For the L_X – M_Δ relation (Figure 3(b)), the re-

sults of fits show $\beta = 1.02 \pm 0.14$ for the whole sample and $\beta = 1.05 \pm 0.12$ for the nonmerging clusters. Compared with the L_X – T_X relation (Figure 3(a)), the dispersion is larger, which may be related to the dispersion of the c_Δ – M_Δ relation (Figure 2). The value of β is consistent with the predictions for $n = -2.5$ in Table 1 and $\beta = 4/3 \approx 1.33$ is clearly rejected.

5. DISCUSSION

We have shown that the suggested new relations for L_X – T_X and L_X – M_Δ once a mass profile is properly taken into account are shallower than the ones predicted from a self-similar model. With the improved understanding of the luminosity-mass relation, we may explore new methods of mass measurements through X-ray luminosity. As shown in Figure 2, a typical scatter of 0.1 dex in the c_Δ – M_Δ relation can produce a scatter of approximately 0.15 dex in the L_X – M_Δ relation. This will account for more than 50% of scatter in observed scatter (e.g. Maughan 2007; Rykoff et al. 2008; Zhang et al. 2008, but see Andreon et al. 2016). This suggests that that the scatter caused by hierarchical structure formation can be comparable to nongravitational effects, and proper modeling of this effect of halo concentrations on the L_X – M_Δ relation will help reduce the scatter and potentially open the path for mass measurements through X-ray luminosity.

If the shallow slopes of the baseline relations are observed, it will be a proof of the hierarchical structure formation. However, real clusters are affected by the aforementioned additional nongravitational effects. For example, the gas fraction of the central region of observed clusters (f_{gas}) is generally smaller than the baryon fraction of the universe (e.g. Vikhlinin et al. 2006; Sun et al. 2009). This is mostly explained as a result of the feedback from AGNs and supernovae, although some of the baryon in clusters is consumed in star formation. The feedback leads to an increase in α and β from the baseline relations. Observations have shown that $\alpha \sim 2.6$ – 3.7 and $\beta \sim 1.6$ – 2.0 (e.g. Edge & Stewart 1991; Ebeling et al. 1996; Markevitch 1998; Arnaud & Evrard 1999; Ikebe et al. 2002; Reiprich & Böhringer 2002; Ettori et al. 2004; Hicks et al. 2008; Zhang et al. 2008; Pratt et al. 2009; Reichert et al. 2011). Some of the studies have shown that even if cluster cores are excised in the analysis, the slopes (e.g. $\alpha = 2.8 \pm 0.2$ and $\beta = 1.63 \pm 0.08$; Maughan 2007) are steeper than those of the baseline relations ($\alpha \sim 1.7$ and $\beta \sim 1.1$ – 1.2). This means that the feedback impacts on the ICM density beyond the cores. If we assume that the indices of the observed relations are $\alpha = 2.9$ and $\beta = 1.8$ and those of the baseline relations are $\alpha = 1.7$ and $\beta = 1.2$, the gas mass fraction at $r < r_s$ should have a temperature and mass dependence of $f_{\text{gas}} \propto T_X^{(2.9-1.7)/2} = T_X^{0.6}$ and $f_{\text{gas}} \propto M_\Delta^{(1.8-1.2)/2} = M_\Delta^{0.3}$, respectively. This is because the typical X-ray emissivity depends on the gas fraction as $\epsilon \propto (\rho_s f_{\text{gas}})^2 \Lambda$. The dependences are steeper than those expected in the simple self-similar model ($f_{\text{gas}} \propto T_X^{(2.9-2)/2} = T_X^{0.45}$ and $f_{\text{gas}} \propto M_\Delta^{(1.8-4/3)/2} \approx M_\Delta^{0.23}$ for $\epsilon \propto (\rho_\Delta f_{\text{gas}})^2 \Lambda$; see Böhringer et al. 2012). It may be easier to confirm the f_{gas} – T_X relation than the f_{gas} – M_Δ relation because the former is steeper. If these dependences are observationally confirmed, they may indirectly prove the shallow

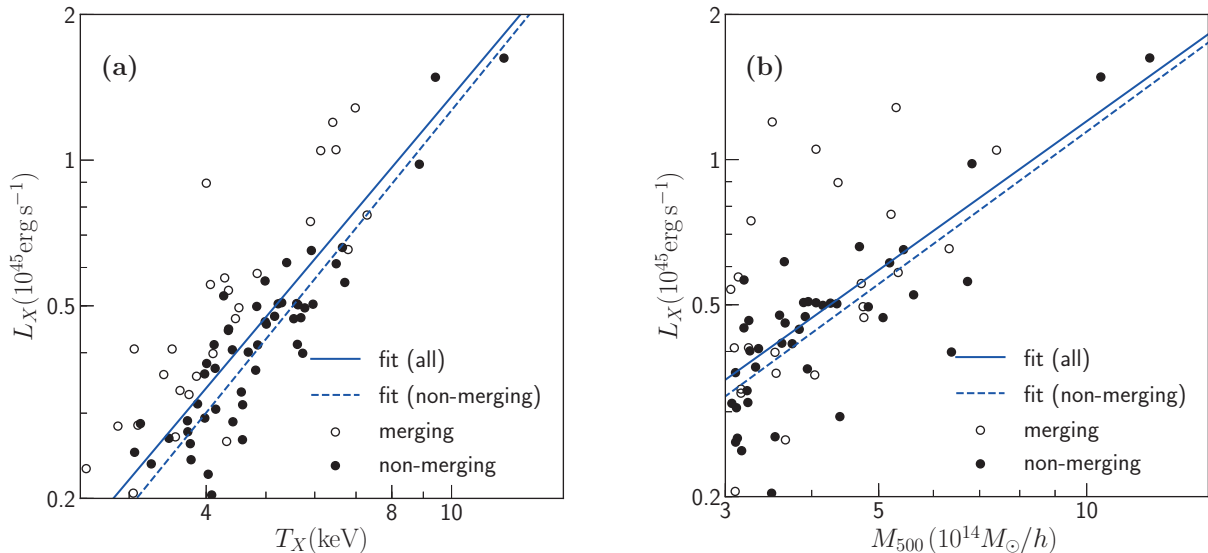


FIG. 3.— Simulated (a) L_X - T_X , and (b) L_X - M_{500} relations at $z = 0$. The open circles are merging clusters and filled circles are others (nonmerging clusters). The best fit for the whole sample and that for the nonmerging clusters are shown by the solid and dashed lines, respectively.

baseline relations and hierarchical structure formation.

The steeper slopes of the $f_{\text{gas}}-T_X$ and $f_{\text{gas}}-M_\Delta$ relations, when the new baseline relations are adopted, can be explained as follows. The new baseline relations reflect that low-temperature clusters have higher concentrations than high-temperature clusters. Thus, the low-temperature clusters have denser gas in the central region compared with those when they have the same concentration as the high-temperature clusters. Thus, stronger feedback and smaller f_{gas} are required for the low-temperature clusters in order to reproduce the observed steep L_X-T_X and L_X-M_Δ relations. In the Appendix, we performed a mock analysis of the $f_{\text{gas}}-T_X$ relation and showed that a sample of ~ 20 clusters is enough to discriminate $f_{\text{gas}} \propto T_X^{0.6}$ from $f_{\text{gas}} \propto T_X^{0.45}$. This method to confirm the hierarchical structure formation may be easier than observationally determining the slope of the $c_\Delta-M_\Delta$ relation because the latter is affected by a large scatter (e.g. Okabe & Smith 2016).

We note that sample selection could be more important than the number of clusters. For example, the observed L_X-T_X and L_X-M_Δ relations could be affected by cluster mergers as well as cool cores. In fact, Maughan et al. (2012) derived a rather small index is of $\alpha = 1.90 \pm 0.14$ for nonmerging clusters with $T_X \gtrsim 4$ keV when the emission from the cool cores are excised, although a similar analysis done by Mahdavi et al. (2013) showed that $\alpha = 2.26 \pm 0.29$.⁵ If the former is the case, it has already suggested the shallower slope of the L_X-T_X relation ($\alpha < 2$), although $\alpha = 2$ cannot be rejected. Since the gas fraction comes close to the universal value for the highest-temperature clusters (e.g. Vikhlinin et al. 2006), the feedback appears to be less effective for

them and the shallower slope is more likely to be realized. Thus, through the L_X-T_X relation for highest-temperature clusters, the hierarchical structure formation could be proved without studying the $f_{\text{gas}}-T_X$ relation. In the near future, *eROSITA* would detect enough numbers of massive or higher-temperature clusters and would enable us to confirm the shallow L_X-T_X and L_X-M_Δ relations with a sufficient degree of accuracy. Follow-up observations with *Chandra* and *XMM-Newton* are also important.

The baseline relations we found should be taken into account especially when the feedback effects are estimated based on the L_X-T_X and/or L_X-M_Δ relations. For example, our discovery indicates that even if the observed index is proven to be $\alpha \sim 2$ or $\beta \sim 4/3$ after considering the effects of cluster mergers and cool cores, it does not mean that those clusters are free from feedback because it is still larger than that for the baseline relation ($\alpha \sim 1.7$ or $\beta \sim 1.1$ – 1.2).

6. SUMMARY

Using the mass dependence of halo concentrations and the fundamental plane relation of galaxy clusters, we have shown that the index of the baseline L_X-T_X relation of clusters, that is, the one when additional physics such as feedback, radiative cooling, and disturbance by cluster mergers are ignored, should be $\alpha \sim 1.6$ – 1.8 . The value is smaller than $\alpha = 2$, which was previously estimated based on a simple self-similar model. For the baseline L_X-M_Δ relation, we showed that the index should be $\beta \sim 1.1$ – 1.2 , which is also smaller than the prediction ($\beta = 4/3$) of the self-similar model. These are because the halo concentration and the characteristic density of clusters increase as the cluster mass decreases in the hierarchical structure formation in a CDM universe. This mass dependence was not considered when the conventional relations of $L_X \propto T_X^2$ and $L_X \propto M_\Delta^{4/3}$ were derived. The new baseline relations would be useful when the feedback effects are estimated based on scaling relations. The baseline relations could be checked by the

⁵ Previous studies that excise cool cores often define the core as the region within $r = \chi r_\Delta$, where χ is the constant (e.g. $\chi = 0.15$ and $\Delta = 500$; Maughan et al. 2012; Mahdavi et al. 2013). If the characteristic density of clusters is r_s rather than r_Δ , the definition of the cool core should also be based on r_s . This redefinition could change the slopes of the observed L_X-T_X and L_X-M_Δ relations, although this is out of the scope of this study.

temperature or mass dependence of gas mass fraction of clusters. We also indicated that the highest-temperature clusters may follow relations close to the new baseline relations if the influences of cool cores and cluster mergers are appropriately treated. This is because the feedback effects are expected to be minimum for those clusters. Near-future cluster surveys (e.g. *eROSITA*) may enable us to confirm the relations more precisely. If they are ac-

tually confirmed, it would be a proof of the hierarchical structure formation.

We thank the anonymous referee, whose comments improved the clarity of this paper. We also thank Hans Böhringer and Daisuke Nagai for useful comments and discussion. This work was supported by MEXT KAKENHI No. 18K03647 (Y.F.).

APPENDIX

MOCK ANALYSIS OF THE GAS FRACTION–TEMPERATURE RELATION

For a quantitative discussion, we perform a simple mock analysis of the $f_{\text{gas}}-T_X$ relation. We create a mock sample of N clusters in a temperature range of $T_{X,\text{min}} \leq T_X \leq T_{X,\text{max}}$. Since the number of clusters with larger temperatures is smaller, we set the temperatures of the clusters following the equation of $T_X = (T_{X,\text{max}} - T_{X,\text{min}})x^2 + T_{X,\text{min}}$, where x is a random number between zero and one, and we assume that $T_{X,\text{min}} = 4$ keV and $T_{X,\text{max}} = 12$ keV. As a result, the expected number of clusters between 10 and 12 keV is about one-fourth of that between 4 and 6 keV. The expected gas fraction at $r < \xi r_s$, where ξ is an appropriate constant, is assumed to be

$$f_{\text{gas}} = f_{\text{gas},10} \left(\frac{T_X}{10 \text{ keV}} \right)^\delta, \quad (\text{A1})$$

where $f_{\text{gas},10}$ is the fraction for clusters with $T_X = 10$ keV, and we assume $f_{\text{gas},10} = 0.1$. The predicted indices for the new and the conventional relations are $\delta = 0.6$ and $\delta = 0.45$, respectively (Section 5). For the conventional relation, we implicitly assume that the halo concentration is independent of the temperature and $r_s \propto r_\Delta$. Clusters distribute along the relation (A1) with an intrinsic scatter. For the gas fraction at $r < r_{500}$ or $r < r_{2500}$, observations have shown that the intrinsic scatter is $\sim 10\%$ and observational uncertainties are much smaller than the intrinsic scatter (e.g. Vikhlinin et al. 2006). As far as we know, there are no previous observational studies on the gas fractions at $r < r_s$. The determination of r_s is rather difficult and the observational uncertainties may be $\sim 30\%$ (e.g. Ettori et al. 2010). Fortunately, the gas fraction is not sensitive to the radius, and even the 30% uncertainties of the radius cause $\lesssim 10\%$ uncertainties for the gas fraction of relaxed clusters (e.g. Figure 6 of Landry et al. 2013). Thus, in addition to the 10% intrinsic scatter, which is given by a random gaussian, we introduce 10% observational uncertainties for f_{gas} . We also assume 3% observational uncertainties for T_X .

For a given index δ , we generate a total of 10^4 realizations of the sample. Using BCES($f_{\text{gas}}|T_X$) regression (Akritas & Bershady 1996), we fit the data with equation (A1) assuming that δ and $f_{\text{gas},10}$ are free parameters, and derive the uncertainties of δ . The results are almost the same if we adopt a BCES orthogonal regression. If we assume that $N = 20$ and $\delta = 0.6$ (the new baseline prediction), the result of the realizations is $\delta = 0.61 \pm 0.07$. This means that $\delta = 0.45$ (the conventional baseline prediction) can be rejected with a sample of $N = 20$ clusters. We note that $\delta = 0.61 \pm 0.10$ for $N = 10$. On the other hand, if we assume that $\delta = 0.45$ and $N = 20$, the result of the realizations is $\delta = 0.45 \pm 0.07$.

The above estimations suggest that the new baseline relation can be confirmed once f_{gas} at $r < \xi r_s$ are derived for not too many clusters. The radius r_s can be determined by fitting an observed mass profile with equation (6). Alternatively, if M_Δ at two different Δ are obtained (say $\Delta = 500$ and 2500), r_s can also be derived from equations (1), (5), and (6).

REFERENCES

- Adami, C., Mazure, A., Biviano, A., Katgert, P., & Rhee, G. 1998, *A&A*, 331, 493
 Akritas, M. G., & Bershady, M. A. 1996, *ApJ*, 470, 706
 Andreon, S., Serra, A. L., Moretti, A., & Trinchieri, G. 2016, *A&A*, 585, A147
 Araya-Melo, P. A., van de Weygaert, R., & Jones, B. J. T. 2009, *MNRAS*, 400, 1317
 Arnaud, M., & Evrard, A. E. 1999, *MNRAS*, 305, 631
 Bertschinger, E. 1985, *ApJS*, 58, 39
 Bhattacharya, S., Habib, S., Heitmann, K., & Vikhlinin, A. 2013, *ApJ*, 766, 32
 Biviano, A., & Salucci, P. 2006, *A&A*, 452, 75
 Böhringer, H., Dolag, K., & Chon, G. 2012, *A&A*, 539, A120
 Borgani, S., Murante, G., Springel, V., et al. 2004, *MNRAS*, 348, 1078
 Bryan, G. L., & Norman, M. L. 1998, *ApJ*, 495, 80
 Child, H. L., Habib, S., Heitmann, K., et al. 2018, *ApJ*, 859, 55
 Correa, C. A., Wyithe, J. S. B., Schaye, J., & Duffy, A. R. 2015, *MNRAS*, 452, 1217
 Diemer, B., & Kravtsov, A. V. 2015, *ApJ*, 799, 108
 Dvorkin, I., & Rephaeli, Y. 2015, *MNRAS*, 450, 896
 Duffy, A. R., Schaye, J., Kay, S. T., & Dalla Vecchia, C. 2008, *MNRAS*, 390, L64
 Ebeling, H., Voges, W., Böhringer, H., et al. 1996, *MNRAS*, 281, 799
 Edge, A. C., & Stewart, G. C. 1991, *MNRAS*, 252, 414
 Eisenstein, D. J., & Hu, W. 1998, *ApJ*, 496, 605
 Enoki, M., Takahara, F., & Fujita, Y. 2001, *ApJ*, 556, 77
 Ettori, S. 2013, *MNRAS*, 435, 1265
 Ettori, S. 2015, *MNRAS*, 446, 2629
 Ettori, S., Gastaldello, F., Leccardi, A., et al. 2010, *A&A*, 524, A68
 Ettori, S., Tozzi, P., Borgani, S., & Rosati, P. 2004, *A&A*, 417, 13
 Fujita, Y., Donahue, M., Ettori, S., et al. 2019, *Galaxies*, 7, 8 (arXiv:1901.00008).
 Fujita, Y., & Takahara, F. 1999, *ApJ*, 519, L51
 Fujita, Y., Umetsu, K., Rasia, E., et al. 2018a, *ApJ*, 857, 118
 Fujita, Y., Umetsu, K., Ettori, S., et al. 2018b, *ApJ*, 863, 37
 Fujita, Y., & Ohira, Y. 2013, *MNRAS*, 428, 599

- Gonzalez, A. H., Sivanandam, S., Zabludoff, A. I., et al. 2013, *ApJ*, 778, 14.
- Hicks, A. K., Ellingson, E., Bautz, M., et al. 2008, *ApJ*, 680, 1022
- Ikebe, Y., Reiprich, T. H., Böhringer, H., Tanaka, Y., & Kitayama, T. 2002, *A&A*, 383, 773
- Kaiser, N. 1986, *MNRAS*, 222, 323
- Kravtsov A. V. 1999, PhD thesis, New Mexico State University
- Kravtsov A. V., Klypin A., Hoffman Y. 2002, *ApJ*, 571, 563
- Landry, D., Bonamente, M., Giles, P., et al. 2013, *MNRAS*, 433, 2790.
- Lanzoni, B., Ciotti, L., Cappi, A., Tormen, G., & Zamorani, G. 2004, *ApJ*, 600, 640
- Ludlow, A. D., Navarro, J. F., Boylan-Kolchin, M., et al. 2013, *MNRAS*, 432, 1103
- Mahdavi, A., Hoekstra, H., Babul, A., et al. 2013, *ApJ*, 767, 116
- Markevitch, M. 1998, *ApJ*, 504, 27
- Maughan, B. J. 2007, *ApJ*, 668, 772
- Maughan, B. J. 2014, *MNRAS*, 437, 1171
- Maughan, B. J., Giles, P. A., Randall, S. W., Jones, C., & Forman, W. R. 2012, *MNRAS*, 421, 1583
- Meneghetti, M., Rasia, E., Vega, J., et al. 2014, *ApJ*, 797, 34
- Navarro, J. F., Frenk, C. S., & White, S. D. M. 1997, *ApJ*, 490, 493
- Nelson K., Lau E. T., Nagai D., Rudd D. H., Yu L. 2014, *ApJ*, 782, 107
- Okabe, N., & Smith, G. P. 2016, *MNRAS*, 461, 3794
- Ota, N., Kitayama, T., Masai, K., & Mitsuda, K. 2006, *ApJ*, 640, 673
- Peebles, P. J. E. 1980, *The large-scale structure of the universe* (Princeton, NJ: Princeton Univ. Press)
- Pratt, G. W., Croston, J. H., Arnaud, M., & Böhringer, H. 2009, *A&A*, 498, 361
- Puchwein, E., Sijacki, D., & Springel, V. 2008, *ApJ*, 687, L53
- Reichert, A., Böhringer, H., Fassbender, R., & Mühlegger, M. 2011, *A&A*, 535, A4
- Reiprich, T. H., & Böhringer, H. 2002, *ApJ*, 567, 716
- Rudd D. H., Zentner A. R., Kravtsov A. V. 2008, *ApJ*, 672, 19
- Rykoff, E. S. and Evrard, A. E. and McKay, T. A. 2008, *MNRAS*, 387, 28
- Schaeffer, R., Maurogordato, S., Cappi, A., & Bernardeau, F. 1993, *MNRAS*, 263, L21
- Sutherland, R. S., & Dopita, M. A. 1993, *ApJS*, 88, 253
- Sun, M., Voit, G. M., Donahue, M., et al. 2009, *ApJ*, 693, 1142
- Verde, L., Haiman, Z., & Spergel, D. N. 2002, *ApJ*, 581, 5
- Vikhlinin, A., Kravtsov, A., Forman, W., et al. 2006, *ApJ*, 640, 691
- Voit, G. M., Bryan, G. L., Balogh, M. L., & Bower, R. G. 2002, *ApJ*, 576, 601
- Wechsler, R. H., Bullock, J. S., Primack, J. R., Kravtsov, A. V., & Dekel, A. 2002, *ApJ*, 568, 52
- Zhang, Y.-Y., Finoguenov, A., Böhringer, H., et al. 2008, *A&A*, 482, 451